Femtosecond laser-induced forward transfer for the deposition of nanoscale, transparent, and solid-phase materials

David P. Banks[*1], Kamal S. Kaur[*1], Christos Grivas[*1], Collin Sones[*1], Pranabendu Gangopadhyay[*1], Charlie Ying[*1], John D. Mills[*1], Sakellaris Mailis[*1], Ioanna Zergioti[*2], Romain Fardel[*3,4], Matthias Nagel[*3], Thomas Lippert[*4], Xu Xu[*5], Stephen P. Banks[*5] and Robert W. Eason[*1]

[*1] *Optoelectronics Research Centre, University of Southampton, Southampton SO17 1BJ UK*
E-mail: dpb@orc.soton.ac.uk
[*2] *Physics Department, National Technical University of Athens, 15780 Zografou, Greece*
[*3] *EMPA, Swiss Federal Laboratories for Materials Testing and Research, Laboratory for Functional Polymers, Überlandstrasse 129, 8600 Dübendorf, Switzerland*
[*4] *Paul Scherrer Institut, General Energy Research Department, 5232 Villigen PSI, Switzerland*
[*5] *Department of Automatic Control and Systems Engineering, University of Sheffield, Sheffield S1 3JD UK*

We present an overview of recent studies of the laser-induced forward transfer (LIFT) process with femtosecond duration pulses. Potential advantages over the technique with nanosecond pulses in terms of depositing smaller features, and transferring solid-phase and transparent materials have been identified and demonstrated experimentally. Nanodroplets of Cr were deposited with diameters as small as 300 nm. The transfer of discs of Cr in solid-phase was achieved using multiple low-energy pulses and simple spatial beam shaping. Oxide and polymer films that are transparent at the laser wavelength have been printed using multiphoton absorption of femtosecond pulses. A femtosecond laser-induced fracturing technique that allows for the non-thermal transfer of bulk transparent materials has been demonstrated. Lastly, LIFT has been used to deposit lines of Ti onto $LiNbO_3$ for subsequent in-diffusion to form waveguides. Single mode operation of the waveguides from 638-1750 nm is observed and losses as low as ~0.8 dB/cm are measured for optimum Ti-transfer conditions.

Keywords: instruction, manuscript, proceedings, LAMP2009, five to ten keywords

1. Introduction

The laser-induced forward transfer (LIFT) technique (as shown in Fig. 1) was initially proposed by Bohandy et al. as a method for microdepositing metal for the repair of damaged photomasks [1]. In LIFT, a thin film of the material to be deposited (the *donor*) is coated onto one face of a transparent support substrate (the *carrier*) and brought into close contact (typically the separation is on the order of a few micrometers) with another substrate (the *receiver*). Transfer of the donor film to the receiver is affected by focusing or demagnifying a laser through the carrier onto the carrier–donor interface. The laser initiates melting [2] or ablation [3] of the donor film, providing the thrust required to propel material to the receiver.

LIFT has been successfully applied for the direct writing of metals and metallic pastes (e.g., see [1,2,4–11]), polymers [12], oxides [13,14], superconductors [15], diamond [16], carbon nanotube field emission cathodes [17], conducting polymers [18], and an adenosine triphosphate sensor fabricated from luciferase [19]. Recently, a number of groups have also investigated the effects of using ultrashort (sub-picosecond) pulses for LIFT (so-called fs-LIFT) [13,20–24]. The majority of work has focused on achieving the smallest possible structures, but fs-LIFT has also been shown to be capable of transferring viable biomaterial [25].

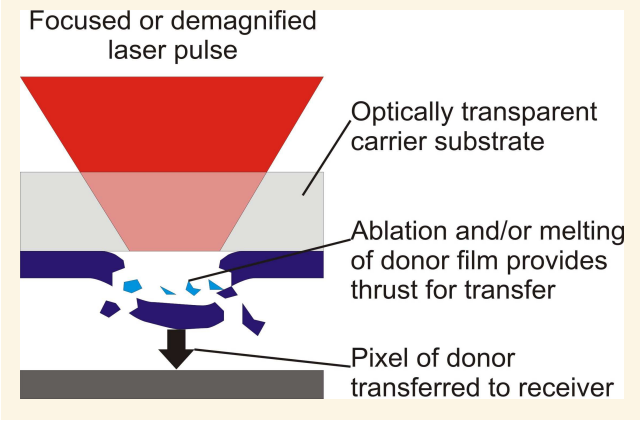

Fig. 1 Schematic of the LIFT process.

In this paper, we present a review of our recent work on the fs-LIFT process. A discussion of the envisaged advantages of using femtosecond over nanosecond pulses for LIFT follows in section 2. The transfer of nanoscale, solid-phase, and transparent materials are the subjects of sections 3, 4, and 5, respectively. A non-thermal, shockwave driven forward transfer technique is described in section 6. Finally, initial results of applying fs-LIFT for patterning metal onto $LiNbO_3$ wafers for subsequent in-diffusion to form waveguides are presented in section 7.

2. The advantages of femtosecond pulses for LIFT

The benefits of using femtosecond pulses for various material processing applications are well known. In particular, the high intensities achievable with femtosecond lasers, results in reduced thermal effects, minimal collateral damage, and ability to directly process virtually any material. For similar reasons, we may expect LIFT to benefit from using femtosecond-duration pulses also.

The most important point concerns the size of the heat-affect zone (HAZ) in targets under laser radiation. With femtosecond lasers, the pulse duration is small compared to characteristic thermal conduction timescales, so the spread of laser energy is governed by electron motion (~100 nm [26]). The size of the HAZ (due to thermal diffusion) at the end of a nanosecond laser pulse can be estimated using [27]

$$l_d = \frac{1}{2}\sqrt{\pi D t_p} \qquad (1)$$

where l_d is the diffusion length, D is the diffusion coefficient and t_p is the pulse duration. As an example, for Cr ($D=28.3\text{x}10^{-6}$ m^2s^{-1}) with 10 ns irradiation, $l_d \sim 0.5$ μm. As a result of this, higher pulse energies are required with longer pulses so thermal damage and the HAZ are increased.

The reduction in thermal effects with ultrashort pulses has implications for LIFT. Firstly, reducing lateral heat diffusion in the donor film has obvious implications for depositing smaller features. Secondly, LIFT can be used to print films that are on the order of a few microns thick, i.e. significantly thicker than the heat diffusion length in the film. Hence, it is possible that a large proportion of the donor is not heated by the laser during transfer, thus allowing for the printing of delicate materials directly, e.g. biomaterials [25].

3. Nanoscale features deposited by fs-LIFT

The transfer of sub-micron droplets via LIFT with nanosecond and femtosecond lasers has been observed by a number of authors [21,22,27,28]. Under optimal conditions, these droplets are typically on the order of 0.5 μm to a few microns in diameter [22,28]. The details of how these droplets form is still not well understood, but it is believed that the donor film melts through [2] and a small amount of evaporation at the constrained interface leads to a bubble forming [28]. It is believed that the bubble growth leads to a flow of molten material towards the centre of the irradiated region and the subsequent expulsion of a jet of material from the bubble surface [29]. Such jets have been observed experimentally for nanosecond-LIFT of liquid films [30]. Droplet formation in the case of films that are solid at room temperature can be attributed to the rapid re-solidification of the jet as it expands and the associated increase in surface tension.

As discussed in section 2, using femtosecond duration pulses for LIFT reduces lateral heat diffusion in the donor film compared to the nanosecond regime. The smaller HAZ results in a smaller melted region and, ultimately, less donor material in the jet. This may result in smaller droplets with shorter duration pulses. It is also important to note that the amount of material in the jet can be reduced by using a thinner donor film. Here we describe the deposition of 300 nm diameter droplets of Cr with fs-LIFT by optimizing the laser fluence and donor thickness. More details of the experiments described in this section can be found in [21].

3.1 Experimental setup

For these experiments, and for all the work described in this paper a Ti:sapphire femtosecond laser system (Coherent Mira9000 and Legend-F) was used. The system produced 2 mJ pulses at a repetition rate of up to 1 kHz at a wavelength of 800 nm. The Gaussian spatial profile pulses were centrally incident on a variable diameter aperture to give an approximately top-hat intensity distribution. An image of the aperture was relayed to the carrier donor interface with a reverse projection, infinity corrected microscope with a tubes lens of focal length 300 mm. An external shutter was used to control laser exposure, and samples were mounted on 3-axis translation stages.

For the nanodroplet experiments, a 100x microscope objective (NA = 0.8, Nikon) with an effective focal length of 10 mm was used, resulting in a demagnification of the aperture of 30x. The aperture diameter was 120 μm, hence the spot size at the carrier-donor interface was 4 μm. For the donor, 30 nm of Cr was thermally evaporated onto the concave face of 1 m focal length BK7 plano-concave lenses. The donor thickness was chosen to slightly greater than the skin depth of Cr at 800 nm so as to be thick enough to prevent laser damage of the receiver, but also thin enough to minimise the amount of melted donor that would form the jet. The plano-concave carriers were used to allow for accurate control of the of the donor-receiver separation. Si wafers were used as receiver substrates. Experiments were carried out in air ambient.

3.2 Nanodroplet transfer

A thorough fluence scan was conducted to identify the threshold fluence for Cr transfer which was found to be 325±5 mJ/cm^2. Above this threshold, a single nanodroplet was obtained per laser shot with a diameter and morphology that was strongly dependent on the applied laser fluence. The graph in Fig. 2 shows how the diameter of these droplets varied with fluence. The SEM micrograph insets A-C illustrate how the morphology of these deposits varied from spherical droplets around the transfer threshold to larger, flatter structures at higher fluence.

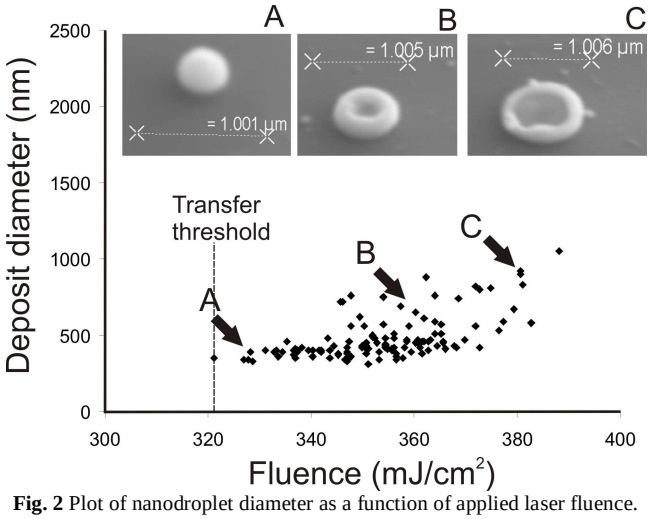

Fig. 2 Plot of nanodroplet diameter as a function of applied laser fluence. SEM insets show typical deposit morphology at the indicated fluence.

At low fluence, from around the transfer threshold to ~345 mJ/cm^2, spherical droplets with diameters from 300-400 nm were reproducibly obtained (Fig. 2 A). Above 345 mJ/cm^2, the variation in the droplet diameter began to increase, although most were still around 400 nm across. However, some were significantly larger, up to around 700-800 nm in diameter. These larger deposits were no longer spherical in shape, but instead exhibited a toroidal profile with a centrally depressed region (Fig. 2 B). For fluences greater than 370 mJ/cm^2, the smallest spherical droplets were no longer obtained. Instead the deposits had large, flattened centres and a thicker rim (Fig. 2 C). The size of these structures varied significantly from 500 nm – 1 μm. Above 390 mJ/cm^2, multiple features were obtained for a single laser shot.

An important point to note is that the volume of material transferred in the droplet did not appear to increase significantly with fluence. Instead, it appeared that the momentum of the droplet upon impact at the receiver was critical in determining the final size and morphology. As the fluence was increased, the droplets impacted with more momentum, which led to a flattening and spreading out of the transferred material. The rapid re-solidification of the droplets upon impact on the 'cold' receiver froze them during the impact process, hence the morphology variation.

3.3 Microarray formation

An obvious application for metallic nanodroplets of 300-400 nm diameter is the formation of plasmonic microarrays. However, this requires sub-micron (and potentially sub-diffraction limit) spacing of the nanodroplets. This presents a problem as droplets must be transferred from previously exposed areas of donor, unless the donor is also moved relative to the receiver between each transfer, which is challenging technically.

To investigate how closely spaced droplets could be placed on the receiver, the laser was raster-scanned across the sample at various speeds to form 1D lines and 2D microarrays of nanodroplets. In the 1D experiments, with a fluence around the transfer threshold, it was found that a minimum spacing of around 1-1.2 μm (i.e. ~1/2 the laser spot radius) was achievable before droplet size and positioning began to vary significantly from shot to shot.

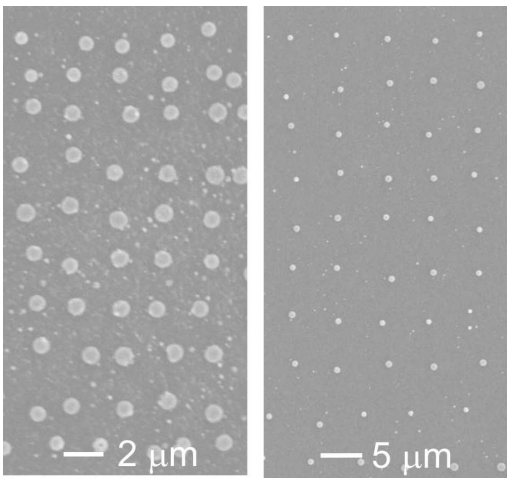

Fig. 3 Microarrays formed with 2 μm and 5 μm periodicity.

Figure 3 shows SEM micrographs of microarrays produced with periodicities of 2 μm (left) and 5 μm (right). It was apparent that, even with a relatively large separation of 2 μm between laser exposures, a significant amount of debris was transferred around the droplets and the array spacing was not constant. This can be attributed to the fact that a given area of donor was exposed to more pulses for a given exposure separation here than in the 1D case. Indeed, it was found that the array spacing had to be increased such that there was no overlap of multiple pulses (i.e. a spacing greater than the laser spot size) for regular arrays of uniform droplets to be produced.

4. Transfer of metallic donors in solid-phase

Despite the great progress made using LIFT techniques in recent years, directly printing segments from 'hard' films, i.e. metals, glasses, crystals, ceramics etc., essentially intact after transfer to maintain the as-deposited properties of the donor is still challenging. Typically LIFT of solid films results in significant melting and shattering of the material during transfer. However, for the LIFT of, for example, single-crystal, oriented, or single domain donor films, or for donors containing pre-fabricated structures, contiguous solid-phase transfer is necessary. Recent results using a triazene polymer sacrificial layer have shown promise in this area [31]; however, there are potential issues of residual-polymer contamination and difficulty in depositing certain donor materials on the heat-sensitive polymer.

As was discussed in section 2, the reduced amount of thermal diffusion in a target illuminated with ultrashort pulses, means that it is possible to heat the constrained donor interface sufficiently to induce some evaporation, without fully melting through the film. In this section, a technique is described that utilizes multiple low energy femtosecond pulses to delaminate and weaken the donor prior to transfer so that melting and shattering is inhibited. This technique is known as Ballistic Laser-Assisted Solid Transfer (BLAST). More details can be found in [32].

4.1 Experimental

The same laser and imaging systems described in section 3.1 were used for BLAST experiments. However, the aperture diameter was increased to 450 μm and a 5x objective with an effective focal length of 30 mm was used, resulting in a spot diameter on the donor of 10 μm.

Cr films 80 and 160 nm thick were evaporated onto fused silica windows for BLAST targets. Si wafers were used as receivers and target-receiver separation was kept around 2 μm by means of Mylar spacers. All results presented here were performed under vacuum at ≈ 0.1mbar, although BLAST has also been observed to work in an ambient atmosphere.

4.2 Ballistic Laser-Assisted Solid Transfer

Figure 4 shows SEM micrographs of structures transferred from the 80 nm Cr donor with 10 pulses and a fluence of 310 mJ/cm^2; note that this fluence was below that measured for the onset of significant melting in Cr in the nanodroplet experiments. Although there was some evidence of melting and ripple structures on the top surface (formally the constrained surface) of the transferred materi-

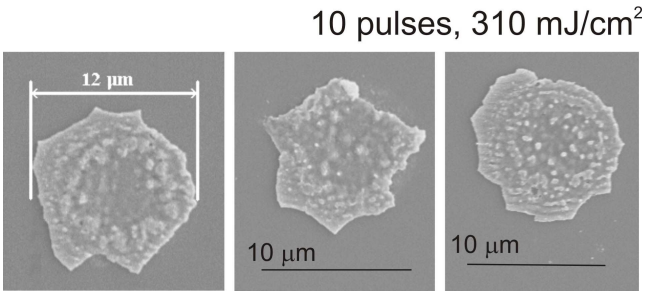

Fig. 4 SEM micrographs of Cr transferred with 10 pulses at 310 mJ/cm^2.

al, the sharp, well-defined edges were clear indicators of transfer in solid-phase. Note that none of the characteristic splatter commonly seen with LIFT depositions was visible with the BLAST deposits and there was no evidence of shattering of the material during transfer.

Observing Fig. 4, it was apparent that the size and shape of the BLAST deposits varied significantly. This was because the film was amorphous and so sheared randomly. To obtain more reproducible deposits, it was necessary to define the area to be transferred by locally weakening the film such that shearing occurred in a pre-defined location. This controlled weakening could be achieved by moving the carrier-donor interface a few microns from the best image plane of the aperture to give a beam with an intense outer ring to define the weak region. More details of the beam shaping principle can be found in [32].

4.3 Results with simple beam shaping

Figure 5 shows SEM micrographs of results from BLAST with spatially shaped pulses. Figure 5(a) shows a Cr pellet transferred from the 80 nm donor film with 10 pulses at 310 mJ/cm^2, i.e. identical printing conditions to those described in the previous section. Comparing Fig. 5(a) with Fig. 4 clearly demonstrates the benefits of using spatially shaped pulses for BLAST. The deposits with spatial shaping were reproducibly circular, with smooth edges, and displayed less surface damage than those with unshaped pulses because the local intensity in the centre was lower in this case due to the mis-imaging.

Figure 5(b) shows a pellet of Cr transferred from the 160 nm film using 10 shaped pulses at 340 mJ/cm^2. Again, the material had clearly been transferred in solid-phase. As the film was slightly thicker in this case, a greater force was required for shearing, hence the edges were not as smooth as with the thinner film. It is interesting to note that, although the average fluence was above the melting threshold of ~325 mJ/cm^2 measured earlier, the local fluence was only sufficient to induce melting around the edges and in the very centre due to the variation of intensity across the imaged spot.

Figure 5(c) shows an SEM micrograph of the 160 nm donor film after exposure to 8 shaped pulses at 340 mJ/cm^2, i.e. insufficient to induce transfer. The effect of the intense outer ring of the shaped laser beam can be clearly seen defining the point of the film that would ultimately shear with sufficient pulses. Note also that there was evidence of melt-through in the centre of the exposed area. This occurred because the very simple beam shaping technique used here meant that there was still a relatively high intensity at this point. This was also the origin of the central damage in 5(b).

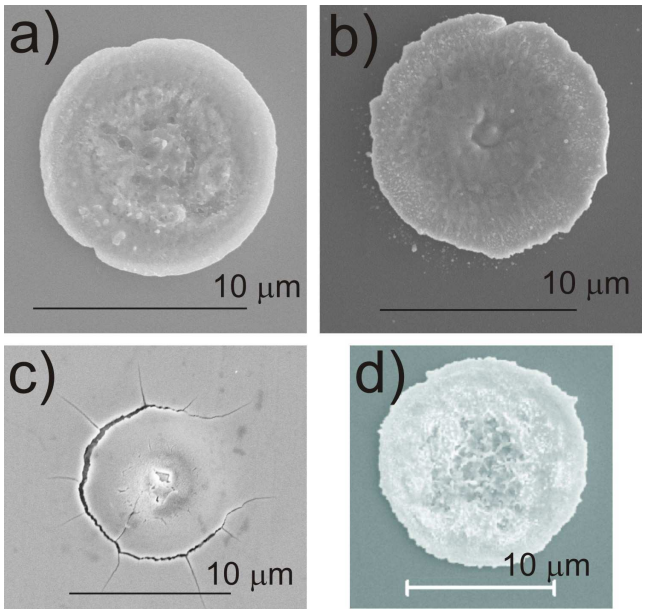

Fig. 5 SEM micrographs of BLAST with shaped pulses. Cr transferred with 10 pulses at 310 mJ/cm^2 from the 80 nm donor film (a), 10 pulses at 340 mJ/cm^2 from 160 nm film (b), the 160 nm Cr donor film with less pulses than the transfer threshold (c) and a Au pellet transferred with 10 pulses at 300 mJ/cm^2 (d).

Figure 5(d) shows another BLAST deposit. In this case the donor film was 150 nm thick Au. The pellet was transferred with 10 pulses at 300 mJ/cm^2. Similar results to those seen with the Cr films were observed; well-defined edges indicated solid-phase transfer although there was some central damage due to the non-optimal beam profile used to do the pre-transfer weakening of the donor.

5. Transfer of transparent polymers and oxide donors

Transferring transparent materials with LIFT is challenging due to the lack of direct absorption of the laser in the donor. Although shorter wavelengths can be used to get direct absorption in many materials, commonly used carrier materials also absorb these wavelengths, rendering them unsuitable for LIFT. Femtosecond LIFT allows for the direct transfer of transparent materials by focusing the laser at the carrier-donor interface to induce multi-photon absorption in the donor just at the interface [33,34].

5.1 Experimental

The laser and imaging setup used for transparent material transfer with fs-LIFT was identical to that used for BLAST, described in section 4.1. Two samples were prepared. The first had a single, 150 nm thick donor film of GdGaO that was transparent to all wavelengths longer than ~300 nm prepared by room temperature PLD. The second included a 100 nm thick dynamic release layer (DRL) [35] of triazene polymer (TP) [36] between the carrier and the GdGaO donor. The TP-DRL was transparent to all wavelengths longer than ~380 nm. Full details of the absorption properties of the DRL and donor films and the sample preparation can be found in [33].

5.2 Transfer results

The threshold for forward transfer of the GdGaO donor was measured to be ~90 mJ/cm^2 with the TP-DRL and

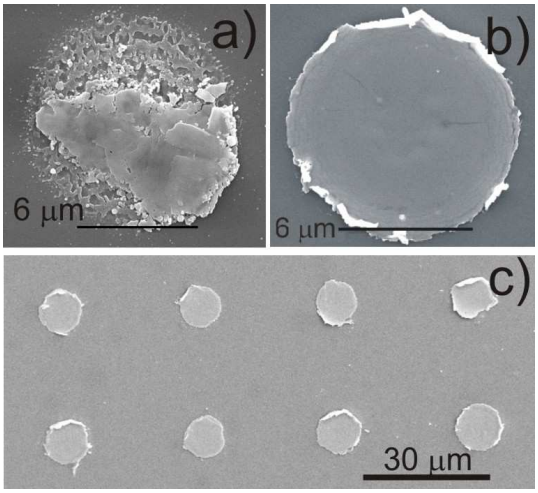

Fig. 6 SEM micrographs of GdGaO transferred using fs-LIFT. Result with only the GdGaO donor (a) and with TP-DRL (b,c).

~110 mJ/cm^2 without it. Figure 6(a) shows an SEM image of transferred GdGaO material using ~120 mJ/cm^2 without the DRL, and Fig. 6(b,c) show SEM micrographs of GdGaO discs deposited with the DRL; fluence ~90–100 mJ/cm^2. The donor-receiver separation was ~50 nm; this could be measured interferometrically as the films were transparent. The benefits of using the TP-DRL for the fs-LIFT of solid material from hard donor films were apparent. Surface profiling of typical discs transferred using the DRL, similar to those in Fig. 6(b,c), indicated that the deposits were reproducibly ~130 nm thick, closely matching the original thickness of the GdGaO donor and indicating that little or no DRL remained on the deposit post-transfer.

A strong dependence of the deposit quality on the donor-receiver separation was observed with the TP-DRL sample [33]. Figure 7 (A-G) shows SEM micrographs of GdGaO deposits obtained with various values of the separation. It was found that the variation of deposit morphology was roughly periodic with a period of ~λ/2. This variation could be explained by considering the intensity of the standing wave that formed in the transparent thin films due to multiple reflections [34].

5.3 Interference and standing waves

As the TP and GdGaO films were transparent to the laser wavelength, multiple reflections occurred off the various interfaces within the sample. The laser coherence length was around 30 μm, which was long compared to the film thicknesses, so interference between the forward and backward propagating waves led to the formation of a standing wave [34].The strongest back-reflection in this setup was off the Si wafer surface; hence, varying the size of the air gap had a significant effect on the local intensities in the film.

The intensity profile of the standing wave could be easily calculated using the refractive indices and thicknesses of the various layers [34]. It was then simple to show that the peak intensity in the donor film varied periodically with the donor-receiver separation with a periodicity of λ/2, as seen in the experiments. The graph in Fig. 7 shows the calculated peak intensity in the donor and DRL layers as a function of the separation assuming an incident fluence of

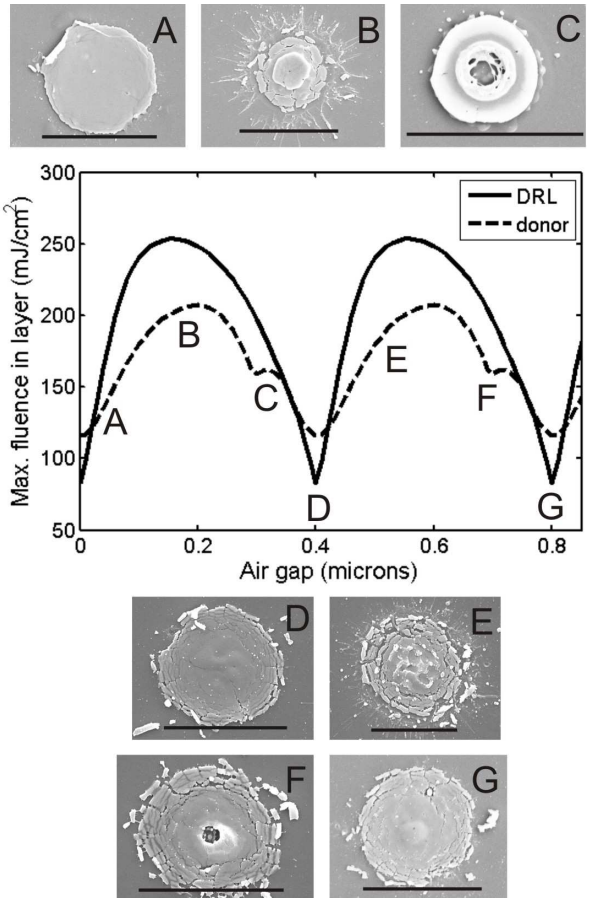

Fig. 7 Plot of the maximum intensity in the DRL (solid line) and donor (dotted line) films as a function of the source-receiver separation. SEM micrographs A-G correspond to the marked points on the plot.

90 mJ/cm^2. The points marked A-G correspond to the SEM micrographs. As can be clearly seen, the most damaged deposits corresponded to values of the separation where the standing wave intensity was maximised, whilst the undamaged deposits were obtained when interference in the donor layer was destructive.

The standing wave was an undesirable side effect of transferring transparent films directly without including an absorber layer. Although it was possible to identify an appropriate combination of film thicknesses and donor-receiver separation that minimised the locally high intensities, the standing wave introduced extra complexity to the technique.

6. Shock-induced forward transfer of fused silica

In the previous section, fs-LIFT of transparent films driven by multi-photon irradiation was presented. Although good quality deposits could be produced by optimising the printing conditions, there are still challenges. Firstly, it was still necessary to directly irradiate the material to be transferred, with the associated thermolytic damage that can occur. Also, because the films are transparent to the laser wavelength, standing waves are produced in the film(s) that can produce local high intensities which can damage the donor.

In this section a non-thermal transfer mechanism is presented that relies on the shockwaves generated by absorption of femtosecond pulses to fracture and transfer trans-

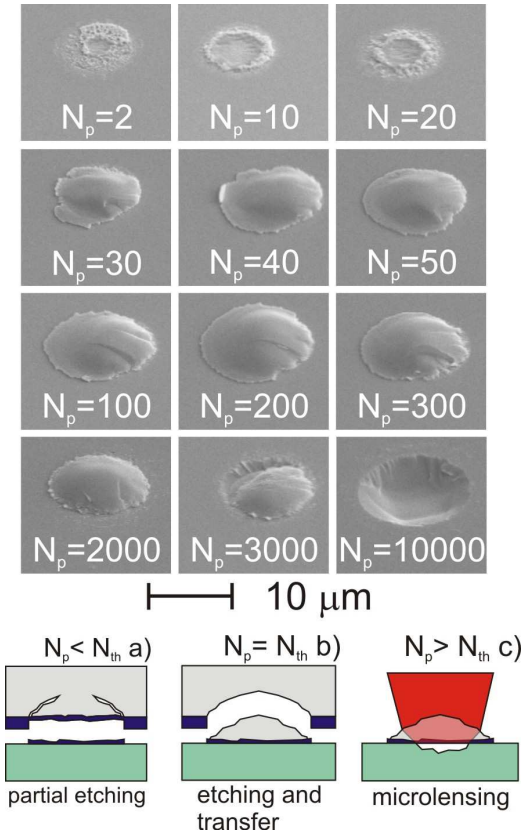

Fig. 8 SEM micrographs of silica deposited onto Si by LISE. Schematics of the envisaged transfer process as a function of pulse number (a-c).

parent materials. This process is different from normal LIFT as it is sections of the carrier substrate that are transferred rather than the donor. This process is known as Laser-Induced Solid Etching (LISE) [37].

6.1 Experimental

For the LISE studies, the experimental setup was identical to that used for BLAST, except that the laser was set to fire at 250 Hz. 80 nm of Cr was again prepared on one face of a fused silica window by thermal evaporation. The Cr-coated face of the silica was pressed into tight contact with the Si receiver. Experiments were carried out in a vacuum chamber at ~0.1 mbar to ensure tight contact between donor and receiver.

The Cr donor was exposed to varying numbers of pulses, N_p, using the external shutter. Absorption of the femtosecond pulses in the Cr caused a large pressure increase that generated strong shockwaves in the silica and Si substrates. The axial strain was greatest at the edge of the irradiated spot so cracks former in the silica in this region. These cracks grew under exposure to multiple pulses until a complete piece of silica was etched out of the carrier in solid-phase. This etched piece could be collected on the Si receiver where re-solidified Cr donor ensured good adhesion. The LISE process is described in more detail in [37].

6.2 LISE of dome-like structures

The first experiments focused on the transfer of individual domes of silica by exposing the Cr to varying numbers of pulses. Figure 8 shows SEM micrographs of sample deposited features of silica on the Si after exposure to varying N_p at a fluence of 400 mJ/cm^2. Note that this fluence was approximately equal to that measured for the onset of evaporation in Cr in the nanodroplet studies in section 3.

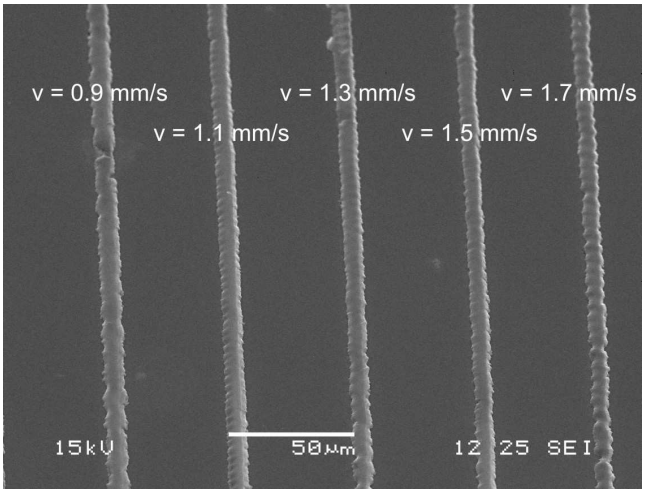

Fig. 9 SEM micrograph of silica lines transferred using LISE.

It was observed that there were two thresholds for transfer; a fluence threshold and a minimum number of pulses, N_{th}. The fluence threshold corresponded approximately to the onset of ablation in the Cr film. The minimum number of pulses was around 20-30. Figure 8 (a-c) show schematics of the envisaged transfer process as N_p was varied relative to N_{th}. With $N_p < N_{th}$ (a) the cracks that formed did not develop sufficiently to etch material from the silica. Instead, just some of the Cr was transferred to the receiver. With $N_p \sim N_{th}$ (b) the silica was cleanly etched and transferred to the Si. With $N_p > N_{th}$ (c), pulses continued to be incident after transfer and could pass through the silica, damaging the underlying Si. Eventually, for $N_p >> N_{th}$ the Si under the deposit was completely machined away and the silica was removed [37].

6.3 LISE of line structures

LISE was also used to deposit lines of silica for potential applications in rib and strip-loaded waveguides [37]. In these experiments, it was found that the threshold fluence for etching (~600 mJ/cm^2) was somewhat higher than in the dome case due to the reduced overlap between multiple pulses. There was also a raster speed threshold (~7 mm/s), akin to the number of pulses threshold in the previous section.

Figure 9 shows typical lines transferred with 700 mJ/cm^2 and varying raster speeds from 0.9-1.7 mm/s, corresponding to separations between successive exposures of 3.5-6.8 μm at 25 Hz (recall that the laser spot size was 10 μm). Similar continuous lines up to 2 μm in height were obtained over a wide range of processing parameters. It was found that the optimal conditions for LISE in terms of producing the smoothest features were high fluence (~0.9-1 J/cm^2) and raster speeds from 1.1 mm/s.

An interesting point to note is that, because the lines were transferred with a pulsed laser, they displayed a periodic variation along the length. This can be seen most clearly in the line produced at 1.7 mm/s in Fig. 9. Such variation may have implications for forming segmented waveguiding structures with novel spectral properties.

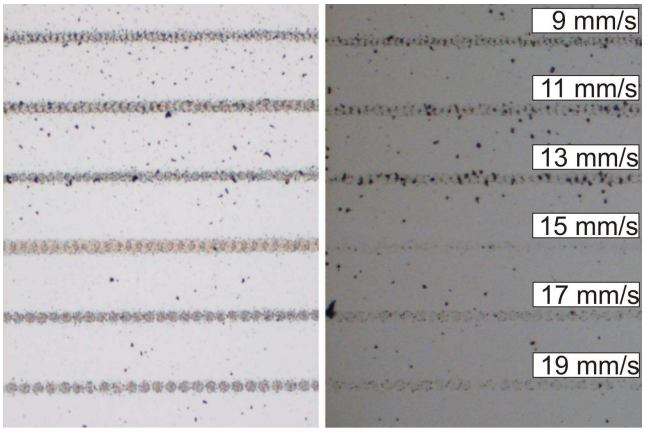

Fig. 10 Optical microscope images of the transferred Ti lines on the $LiNbO_3$ surface pre- (left) and post- (right) in-diffusion.

7. LIFT for rapid prototyping of waveguides

The key advantages of the LIFT technique are speed, simplicity, and versatility. In this section, results combining LIFT of Ti with subsequent in-diffusion into $LiNbO_3$ for the rapid prototyping of in-diffused Ti:$LiNbO_3$ waveguides are presented.

In-diffusion is an attractive technique for forming waveguides due to the high refractive index contrasts that can be achieved relatively easily. However, it has been considered that the deposited metal should be extremely uniform prior to in-diffusion for good waveguides to be formed. As such, complex lithographic processing is normally applied. Here we demonstrate that good quality waveguides can be produced from metal deposited by fs-LIFT despite the inherent variation of metal thickness after transfer. It appears that the in-diffusion process smoothes out the variation of metal thickness.

7.1 Experimental

The laser and imaging setup were the same as in the previous sections. The laser repetition rate was again 250 Hz. Donor films of 100 nm thick Ti were prepared by e-beam evaporation on fused silica windows. 1" square, 0.5mm thick $LiNbO_3$ wafers were used as receivers. LIFT was performed in air ambient onto the –z face of the $LiNbO_3$ wafers. Ti in-diffusion was performed in a furnace at 1060 °C with a ramp rate of 4 °C/min. The samples were diffused in a dry O_2 atmosphere with a flow rate of 0.5 L/min.

7.2 Results

Figure 10 shows optical microscope images of Ti lines transferred on $LiNbO_3$ with fluence of ~350 mJ/cm^2 with the indicated raster speeds. The images show the –z face before (left) and after (right) in-diffusion. As can be seen, for slower scan speeds, a large amount of debris was produced due to the overlap of successive pulses; this debris was still present after in-diffusion. Once the raster speed was increased above ~15 mm/s such that there was no overlap, there was very little debris and the transferred material was almost completely in-diffused.

The waveguiding properties of the in-diffused structures were investigated at 632.8 and 1532 nm. The waveguides were all multi-mode at 632.8 nm, but single-mode operation was observed for all the structures, even

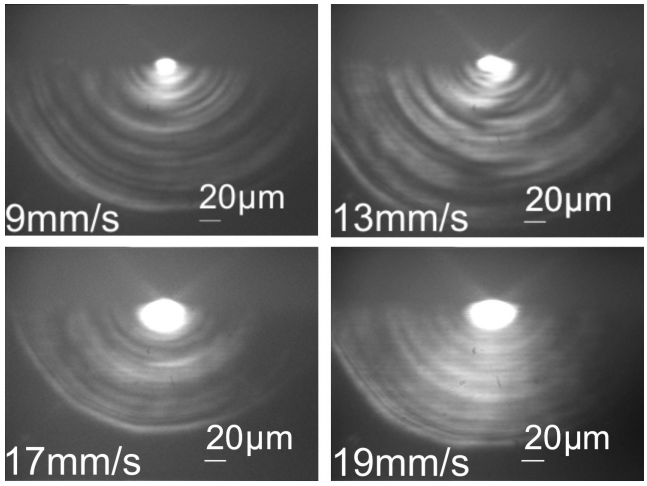

Fig. 11 Images showing the mode profiles of in-diffused waveguides.

those with exhibiting significant surface debris, at 1532nm. Figure 11 shows images of the output mode profiles of the in-diffused waveguides produced at 9, 13, 17, and 19 mm/s shown in Fig. 10. The most striking observation was the significant dependence of the size of the mode profile on the raster speed. This occurred because the average refractive index of the waveguide decreased with increasing raster speed.

The losses of the waveguides were measured using cut-back methods. There was quite a significant variation in the measured values of the loss; the key parameter appeared again to be the raster speed. The lowest losses were measured to be ~0.8 dB/cm with waveguides written at 11 and 13 mm/s. This observation was somewhat surprising because these waveguides suffered from significant surface debris (see Fig. 10) which normally increases the loss in buried waveguides.

The spectral properties of the waveguides were measured using white-light spectral analysis. The waveguides were measured to be single-mode across a broad spectral range from 639-1750 nm.

These results demonstrated that combining the versatility of LIFT with the high refractive index contrasts achievable with in-diffusion is a viable method of producing low-loss waveguides. Furthermore, as the technique is direct-write, it offers the capability to produce devices with novel spectral properties quickly and simply.

8. Conclusions

In conclusion, a number of aspects of the femtosecond LIFT process have been studied in detail. Advantages over the process with nanosecond LIFT in terms of reducing both the size of features that can be produced, and the amount of photolytic and thermolytic damage suffered by the donor, due to the reduced thermal effects with femtosecond pulses have been identified.

Experimentally, fs-LIFT has been used to deposit droplets of Cr 300 nm in diameter, significantly smaller than those previously reported. It is believed that the reason such small droplets could be obtained was in part due to a reduction in lateral heat diffusion in the donor from using femtosecond pulses, and also by using an ultra-thin donor film to reduce the amount of material irradiated by the laser.

The transfer of Cr in solid-phase without shattering has

been achieved using multiple low energy pulses first to delaminate the donor from the carrier in the irradiated region, and then shear it to transfer a pellet. This technique benefits from the reduced thermal diffusion through the donor film to prevent excessive melt-through and facilitate solid-phase transfer. Simple spatial shaping of the laser was incorporated to improve the reproducibility of the transferred features. The shaping resulted in an intense outer ring region that caused significant melting of the donor and encouraged shearing at a desired point, rather than randomly as occurred with the unshaped pulses.

A major advantage of the fs-LIFT technique is the ability to directly print transparent materials without incorporating an absorber layer that can cause post-transfer contamination. Transparent material transfer has been demonstrated using polymer and oxide thin films and excellent quality depositions could be obtained under optimal printing conditions. However, an extra challenge was found that a standing wave was produced in the films if all layers were transparent. Hence, the experimental parameters had to be carefully controlled to prevent unintentional locally high intensities being generated that damaged the donor material. This introduced an extra degree of complexity to the technique but did not prohibit the transfer of undamaged material.

A non-thermal forward transfer technique has been demonstrated that is also applicable for patterning transparent materials. The technique relies on femtosecond generated shockwaves to fracture a bulk transparent substrate and transfer complete pieces in solid-phase. Initial results have demonstrated that LISE is capable of printing continuous lines a couple of microns high. However, there are still major technical challenges to be addressed if the technique is to be used for applications such as rib waveguide formation. Firstly, it will be necessary to eliminate the residual absorber layer between the transferred material and the underlying substrate.

Finally, we have demonstrated that the strengths of the LIFT technique can be combined with those of in-diffusion to form low-loss waveguides. The in-diffusion process appears to smooth out the variation in metal layer thickness, contrary to conventional wisdom on forming in-diffused waveguides. Using this technique we have been able to define waveguides with losses as low as 0.8 dB/cm that are single mode over a wide spectral range. This method for forming in-diffused waveguides is particularly attractive due to its ability to control the waveguide properties through the direct-write LIFT process.

Acknowledgments

The authors are grateful to the Engineering and Physical Sciences Research Council, UK, for research funding under grant EP/C515668/1. The financial support of the Swiss National Science Foundation is also acknowledged.

References

[1] J. Bohandy, B. Kim, and F. Adrian, "Metal deposition from a supported metal film using an excimer laser," *J. Appl. Phys.* **60**, 1538–1539 (1986).

[2] D. Willis and V. Grosu, "Microdroplet deposition by laser-induced forward transfer," *Appl. Phys. Lett.* **86**, 244103 (2005).

[3] F. Adrian, J. Bohandy, B. Kim, A. Jette, and P. Thompson, "A study of the mechanism of metal deposition by the laser-induced forward transfer process," *J. Vac. Sci. Technol. B* **5**, 1490–1494 (1987).

[4] Z. Toth, Z. Kantor, P. Mogyorosi, and T. Szorenyi, "Surface patterning by pulsed laser induced transfer of metals and compounds," *Proc. SPIE* **1279**, 150–157 (1990).

[5] H. Esrom, J. Zhang, U. Kogelschatz, and A. Pedraza, "New approach of a laser-induced forward transfer for deposition of patterned thin metal films," *Appl. Surf. Sci.* **86**, 202–207 (1995).

[6] I. Zergioti, D. Papazoglou, A. Karaiskou, C. Fotakis, E. Gamaly, and A. Rode, "A comparative schlieren imaging study between ns and sub-ps laser forward transfer of Cr," *Appl. Surf. Sci.* **208–209**, 177–180 (2003).

[7] Y. Nakata and T. Okada, "Time-resolved microscopic imaging of the laser-induced forward transfer process," *Appl. Phys. A* **69**, S275–S278 (1999).

[8] R. Bahnisch, W. Gross, and A. Menschig, "Single-shot, high repetition rate metallic pattern transfer," *Microelectron. Eng.* **50**, 541–546 (2000).

[9] B. Tan, K. Venkatakrishnan, and K. Tok, "Selective surface texturing using femtosecond pulsed laser induced forward transfer," *Appl. Surf. Sci.* **207**, 365–371 (2003).

[10] L. Landstrom, J. Klimstein, G. Schrems, K. Piglmayer, and D. Bauerle, "Single-step patterning and the fabrication of contact masks by laser-induced forward transfer," *Appl. Phys. A* **78**, 537–548 (2004).

[11] A. Piqué, D.B. Chrisey, R.C.Y. Auyeung, J. Fitz-Gerald, H.D. Wu, R.A. McGill, S. Lakeou, P.K. Wu, V. Nguyen and M. Duignan, "A novel laser transfer process for direct writing of electronic and sensor materials," *Appl. Phys. A* **69**, S279-S284 (1999).

[12] I. Lee, W. Tolbert, D. Dlott, M. Doxtader, D. Foley, D. Arnold and E. Ellis, "Dynamics of laser ablation transfer imaging investigated by ultrafast microscopy," *J. Imaging Sci. Technol.* **36**, 180–187 (1992).

[13] I. Zergioti, S. Mailis, N. Vainos, P. Papakonstantinou, C. Kalpouzos, C. Grigoropoulos and C. Fotakis, "Microdeposition of metal and oxide structures using ultrashort laser pulses," *Appl. Phys. A* **66**, 579–582 (1998).

[14] H. Sakata, S. Chakraborty, E. Yokoyama, M. Wakaki, and D. Chakravorty, "Laser-induced forward transfer of TiO-Au nanocomposite films for maskless patterning," *Appl. Phys. Lett.* **86**, 114104 (2005).

[15] E. Fogarassy, C. Fuchs, F. Kerherve, G. Hauchecorne, and J. Perriere, "Laser-induced forward transfer of high-T_c YBaCuO and BiSrCaCuO superconducting thin films," *J. Appl. Phys.* **66**, 457–459 (1989).

[16] S. Pimenov, G. Shafeev, A. Smolin, V. Konov and B. Vodolaga, "Laser-induced forward transfer of ultra-fine diamond particles for selective deposition of diamond films," *Appl. Surf. Sci.* **86**, 208–212 (1995).

[17] S. Chang-Jian, J. Ho, J. Cheng and C. Sung, "Fabrication of carbon nanotube field emission cathodes in patterns by a laser transfer method," *Nanotechnology* **17**, 1184–1187 (2006).

[18] B. Thomas, A. Alloncle, P. Delaporte, M. Sentis, S. Sanaur, M. Barret and P. Collot, "Experimental investigations of laser-induced forward transfer process of or-

ganic thin films," *Appl. Surf. Sci.* **254**, 1206–1210 (2007).

[19] Y. Tsuboi, Y. Furuhata and N. Kitamura, "A sensor for adenosine triphosphate fabricated by laser-induced forward transfer of luciferase onto a poly(dimethylsiloxane) microchip," *Appl. Surf. Sci.* **253**, 8422–8427 (2007).

[20] L. Yang, C. Wang, X. Ni, Z. Wang, W. Jia and L. Chai, "Microdroplet deposition of copper film by femtosecond laser-induced forward transfer," *Appl. Phys. Lett.* **89**, 161110 (2006).

[21] D. Banks, C. Grivas, J. Mills, I. Zergioti and R. Eason, "Nanodroplets deposited in microarrays by femtosecond Ti:sapphire laser induced forward transfer," *Appl. Phys. Lett.* **89**, 193107 (2006).

[22] S. Bera, A. Sabbah, J. Yarbrough, C. Allen, B. Winters, C. Durfee and J. Squier, "Optimization study of the femtosecond laser-induced forward-transfer process with thin aluminium films," *Appl. Opt.* **46**, 4650–4659 (2007).

[23] C. Germain, L. Charron, L. Lilge and Y. Tsui, "Electrodes for microfluidic devices produced by laser induced forward transfer," *Appl. Surf. Sci.* **253**, 8328–8333 (2007).

[24] F. Claeyssens, A. Klini, A. Mourka and C. Fotakis, "Laser patterning of Zn for ZnO nanostructure growth: Comparison between laser induced forward transfer in air and in vacuum," *Thin Solid Films* **515**, 8529–8533 (2007).

[25] I. Zergioti, A. Karaiskou, D. Papazoglou, C. Fotakis, M. Kapsetaki and D. Kafetzopoulos, "Time resolved schlieren study of sub-pecosecond and nanosecond laser transfer of biomaterials," *Appl. Surf. Sci.* **247**, 584–589 (2005).

[26] J. Hohlfeld, S.S. Wellershoff, J. Gudde, U. Conrad, V. Jahnke and E. Matthias, "Electron and lattice dynamics following optical excitation of metals," *Chem. Phys.* **251**, 237-258 (2000).

[27] P. Papakonstantinou, N. Vainos and C. Fotakis, "Microfabrication by UV femtosecond laser ablation of Pt, Cr and indium oxide thin films," *Appl. Surf. Sci.*, **151**, 159-170 (2009).

[28] A. Narazaki, T. Sato, R. Kurosaki, Y. Kawaguchi and H. Niino, "Nano- and microdot array formation of $FeSi_2$ by nanosecond excimer laser-induced forward transfer," *Appl. Phys. Exp.* **1**, 057001 (2008).

[29] A. Pearson, E. Cox, J.R. Blake and S.R. Otto, "Bubble interactions near a free surface," ***Eng. Anal. Bound. Elem.* 28 (4)**, 295-313 (2004).

[30] M. Duocastella, J.M. Fernández-Pradas, P. Serra and J.L. Morenza, "Jet formation in the laser forward transfer of liquids," *Appl. Phys. A* **93**, 453-456 (2008).

[31] R. Fardel, M. Nagel, F. Nüesch, T. Lippert and A. Wokaun, "Fabrication of organic light-emitting diode pixels by laser-assisted forward transfer," *Appl. Phys. Lett.* **91**, 061103 (2007).

[32] D. Banks, C. Grivas, I. Zergioti and R. Eason, "Ballistic laser-assisted solid transfer (BLAST) from a thin film precursor," *Opt. Express* **16**, 3249-3254 (2008).

[33] D.P. Banks, K. Kaur, R. Gazia, R. Fardel, M. Nagel, T. Lippert and R.W. Eason, "Triazene photopolymer dynamic release layer-assisted femtosecond laser-induced forward transfer with an active carrier substrate," *Europhys. Lett.* **83**, 38003 (2008).

[34] D.P. Banks, K.Kaur and R.W. Eason, "Influence of optical standing waves on the femtosecond laser-induced forward transfer of transparent thin films," *Appl. Opt.* **48 (11)**, 2058-2066 (2009).

[35] W. Tolbert, I. Lee, M. Doxtader, E. Ellis and D. Dlott, "High-speed color imaging by laser ablation transfer with a dynamic release layer: fundamental mechanisms," *J. Imag. Sci. Tech.* **37(4)**, 411-421 (1993).

[36] M. Nagel, R. Hany, T. Lippert, M. Molberg, F.A. Nüesch and D. Rentsch, "Aryltriazene photopolymers for UV-laser applications: Improved synthesis and photodecomposition study," *Macromol. Chem. Phys.* **208**, 277-286 (2007).

[37] D.P. Banks, K.S. Kaur and R.W. Eason, "Etching and forward transfer of fused silica in solid-phase by femtosecond laser-induced solid etching (LISE)," *Appl. Surf. Sci., Accepted for publication* (2009).